ACS APPLIED ENERGY MATERIALS
Cite This: ACS Appl. Energy Mater. 2019, 2, 7980−7990
Article
www.acsaem.org

Composite Polymer Electrolyte for Highly Cyclable Room-Temperature Solid-State Magnesium Batteries

Ramasubramonian Deivanayagam,[†] Meng Cheng,[†] Mingchao Wang,[‡] Vallabh Vasudevan,[‡] Tara Foroozan,[†] Nikhil V. Medhekar,[‡] and Reza Shahbazian-Yassar*[,†]

[†]Department of Mechanical and Industrial Engineering, University of Illinois at Chicago, Chicago, Illinois 60607, United States
[‡]Department of Materials Science and Engineering, Monash University, Clayton, VIC 3800, Australia

Supporting Information

ABSTRACT: Developing an electrolyte candidate with a wide voltage window, highly reversible cycling with Mg-metal anode, and without the use of any flammable solvents is a major challenge for rechargeable Mg batteries. While there have been several reports on Mg^{2+}-conducting polymer electrolytes with high ionic conductivities, studies to determine their cycling performance and Mg-deposition overpotentials have been scarce. Here, we report a composite polymer electrolyte that exhibits a highly reversible cycling with Mg-metal anode at room temperature. The synthesized polymer electrolyte has a high conductivity of 0.16 mS cm^{-1} at room temperature, and the galvanostatic cycling tests of Mg | Mg symmetric cells reveal that the reversible Mg deposition/stripping occurs at low overpotentials of 0.1−0.3 V for up to 400 cycles. The cycling stability of this composite polymer electrolyte is unprecedented among ambient-temperature solid-state Mg electrolytes, and the observed overpotential values are even comparable to those of the present state-of-the-art liquid electrolytes.

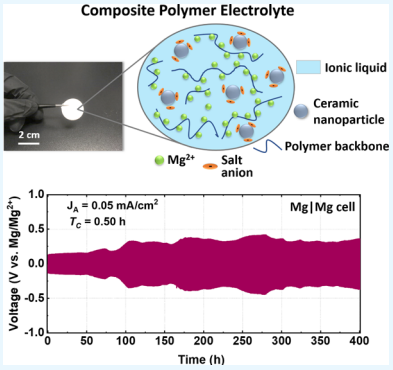

KEYWORDS: *multivalent ion batteries, magnesium batteries, solid polymer electrolyte, composite polymer, galvanostatic cycling, low overpotential*

INTRODUCTION

There has been an active interest in battery systems based on multivalent ions such as Mg^{2+}, Zn^{2+}, Ca^{2+}, and Al^{3+} ions.[1−4] The key motivation behind multivalent-ion battery research is that it offers the promise of obtaining two or three times the energy density of monovalent-ion systems such as Li-ion and Na-ion batteries.[1] Several prototypes have already been developed for Mg-ion, Zn-ion, Ca-ion, and Al-ion batteries.[1,5−7] Among these, magnesium (Mg) batteries are of particular interest owing to the low propensity of Mg-metal to form dendrites, which enables the use of the Mg-metal itself as the battery anode.[8,9] This is an important advantage considering that dendrite growth in Li-metal has been the most prominent detrimental factor preventing the use of Li-metal anodes in Li-ion batteries. Mg-metal also possesses a superior volumetric capacity (3862 mAh cm^{-3}) in comparison to Li-metal (2062 mAh cm^{-3}). Coupling these advantages with the fact that magnesium is a highly abundant metal (eighth most abundant element), Mg batteries are being projected as the most feasible multivalent-ion battery system to complement the role of Li-ion batteries in practical applications.[10−12] However, there are significant challenges that need to be resolved before attempting to commercialize Mg batteries.[13]

Specifically, two important limitations hinder the development of high-energy-density Mg batteries. First, the choice of Mg battery cathode candidates, with a high specific capacity and capacity retention, is limited in comparison with Li and Na battery systems. This is mainly due to slow solid-state diffusion of Mg^{2+} ions.[14] Second, there is a lack of compatible electrolytes that support high cyclability with Mg-metal and simultaneously possess a high oxidative stability (voltage window).[12,15] This limitation has also affected the research progress in magnesium intercalation (cathode) materials.[16] With the limited development of electrolytes with high voltage windows, it has been challenging to experimentally identify and evaluate the reversibility of prospective cathode materials for Mg-ion batteries.[17,18] The Grignard reagents that are compatible with the Mg-metal anode possess a low oxidative stability of <1.5 V, which is not high enough to investigate possible cathode candidates for Mg-ion batteries.[15,19] To improve the oxidative stability and the kinetics of Mg^{2+} ions within the electrolyte, several liquid electrolytes were designed with organometallic reagents dissolved in solvents such as tetrahydrofuran (THF), diglyme, and tetraglyme.[20,21] Although these electrolytes exhibit a high degree of reversibility and oxidative stability, the use of flammable, volatile ethereal solvents such as THF poses a safety risk.[22] This conflicts with the notion of projecting Mg-metal batteries as a safer alternative to Li-metal batteries. Therefore, it is also important to choose electrolyte constituents that do not

Received: July 26, 2019
Accepted: October 22, 2019
Published: October 22, 2019

DOI: 10.1021/acsaem.9b01455
ACS Appl. Energy Mater. 2019, 2, 7980−7990

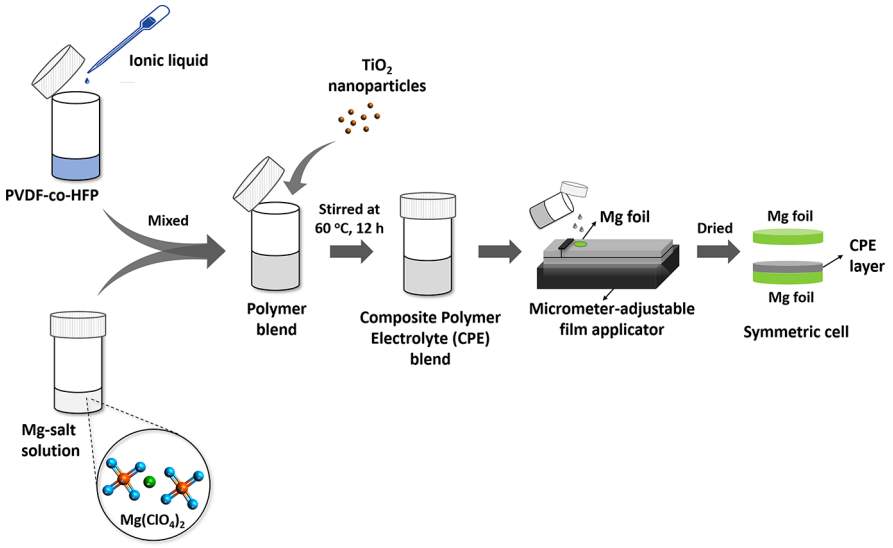

Figure 1. Procedure to synthesize the composite polymer electrolyte (CPE) blend and to coat the CPE blend onto Mg foil using a micrometer-adjustable film applicator.

compromise the superior safety aspects of the Mg-metal anode.[12]

Polymers like poly(ethylene) oxide (PEO) and polyvinylidene fluoride (PVdF) have been known for a long time to be robust, conductive media for Li-ion battery electrolytes.[23−26] It has been proposed that their mechanical properties and conductivities could be further enhanced by incorporating ceramic fillers such as SiO_2, MgO, Al_2O_3, and TiO_2 into the polymers.[27−31] An effective use of these polymers can eliminate the need of using liquid solvents for dissolving the salts in a battery electrolyte. Following their successful integration into Li-battery systems, there have been several reports on Mg-ion-conducting polymer electrolytes possessing high ionic conductivities.[32−38] Chusid et al.[32] developed a gel-type polymer electrolyte consisting of a Mg organohaloaluminate salt: $Mg(AlCl_2\text{-}EtBu)_2$ (where Et: ethyl, Bu: butyl), PVdF, and tetraglyme, which acted as the plasticizer. This gel electrolyte had a high ionic conductivity of 3.7 mS cm^{-1} and exhibited a reversible cycling with the Chevrel-phase Mo_6S_8 cathode for several cycles. Pandey et al.[33] developed a gel polymer electrolyte with magnesium perchlorate ($Mg(ClO_4)_2$), poly(vinylidene fluoride-co-hexafluoropropylene) (PVdF-HFP), MgO nanoparticles, and organic solvents such as ethylene carbonate (EC), propylene carbonate (PC), and tetrahydrofuran (THF) incorporated in the polymer blend. Although a high ionic conductivity of 8 mS cm^{-1} was observed in this gel polymer, no cycling data were reported. There have been other reports on polymer electrolytes based on $Mg(ClO_4)_2$/PVdF-HFP using conventional carbonate-based solvents such as EC and PC reporting conductivities in the range of 10^{-3} S cm^{-1}.[39−41] Alternatively, ionic liquids such as 1-ethyl-3-methylimidazolium trifluoromethanesulfonate (EMITF) has also been used as the plasticizer for $Mg(ClO_4)_2$/PVdF-HFP-based polymer electrolytes.[38] However, the cycling performance of such gel−polymer electrolytes against the Mg-metal anode needs improvement. More recently, Shao et al.[37] developed a polymer nanocomposite electrolyte made of $Mg(BH_4)_2$, PEO, and MgO nanoparticles without the use of any plasticizer or solvent. When this polymer electrolyte was coupled with a Chevrel-phase Mo_6S_8 cathode, the Mg-metal cells exhibited a highly stable specific capacity for 150 cycles. However, these cycling experiments were conducted at a high temperature of 100 °C. Although the cycling performance is impressive, this high-temperature requirement might make it challenging to incorporate this polymer electrolyte in practical applications. In order to project Mg batteries for practical applications, it is important to develop electrolytes that are capable of Mg plating/stripping at ambient temperature.[12]

Here we report a PVdF-HFP-based composite polymer electrolyte (CPE) with $Mg(ClO_4)_2$ salt, 1-butyl-1-methylpyrrolidinium bis(trifluoromethyl)sulfonyl imide (Pyr_{14}-TFSI) ionic liquid, and TiO_2 ceramic nanoparticle fillers for application in solid-state Mg-metal batteries at room temperature. We find that the CPE exhibits a high cyclability with a Mg-metal anode at room temperature. Galvanostatic cycling of symmetric Mg | Mg two-electrode cells reveals smooth plating/stripping profiles with low deposition/dissolution overpotentials in the range of 0.08−0.30 V at current densities of 0.05 and 0.10 mA cm^{-2}. Moreover, the CPE exhibits a high conductivity of 0.16 mS cm^{-1} at room temperature. Raman spectra of the polymer composites obtained at different stages of the synthesis reveal a high degree of salt dissociation, which was further confirmed through classical molecular dynamics simulations. Our casting technique using a micrometer-adjustable film applicator allows the control of the thickness of the electrolyte layer with a high precision. For the cycling tests, the thickness of the electrolyte was controlled to be within 60−80 μm. The high cyclability of Mg-metal cells coupled with such low deposition potentials appears promising toward the development of safe, long-life, solid-state Mg batteries.

■ RESULTS AND DISCUSSION

Figure 1 depicts the procedure for synthesizing the composite polymer electrolyte (CPE). A detailed synthesis procedure is given in the Experimental Section. The CPE blend consists of magnesium perchlorate ($Mg(ClO_4)_2$) salt dispersed in a mixture of poly(vinylidene fluoride-co-hexafluoropropylene) (PVdF-HFP) polymer base, 1-butyl-1-methylpyrrolidinium bis(trifluoromethyl)sulfonyl imide (Pyr_{14}-TFSI) ionic liquid, and TiO_2 ceramic nanoparticle fillers. The polymer PVdF-HFP

DOI: 10.1021/acsaem.9b01455
ACS Appl. Energy Mater. 2019, 2, 7980−7990

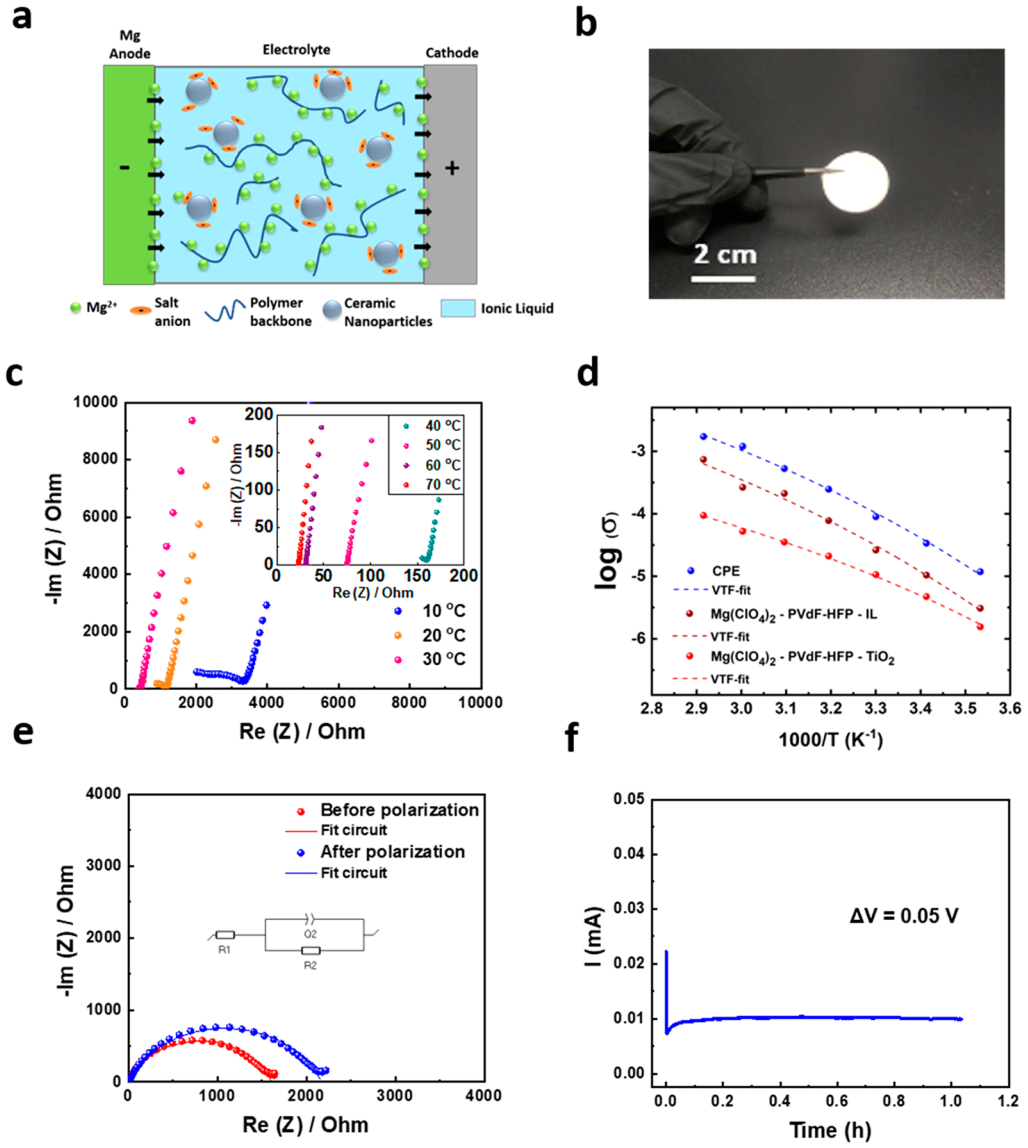

Figure 2. (a) Schematic of a composite polymer electrolyte depicting the role of its constituents in Mg-ion conduction. (b) Digital image of the dried CPE held by a tweezer. (c) Nyquist plots obtained at different temperatures between 10 and 70 °C with the CPE sandwiched between two stainless-steel electrodes. The inset shows the plots obtained between 40 and 70 °C. (d) Temperature−conductivity plots of the CPE, $Mg(ClO_4)_2$−PVdF-HFP−IL, and $Mg(ClO_4)_2$−PVdF-HFP−TiO_2 samples and their corresponding VTF−fit curves. (e) Nyquist plots of a Mg | CPE | Mg cell before and after DC polarization. (f) Time−current plot of the DC polarization experiment carried out on the symmetric Mg | CPE | Mg cell.

is known for its superior mechanical properties and high electrochemical stability.[42,43] Addition of ionic liquids to polymer electrolytes is known to improve the safety, high-temperature stability, and conductivity of polymer electrolytes.[44,45] Here, the ionic liquid, Pyr_{14}-TFSI, was chosen to leverage its additional advantage of being able to act as a cosolvent for Mg salts.[46,47] To improve the mechanical properties and conductivities of Mg^{2+}-conducting polymer electrolytes, addition of nanosized ceramics such as MgO, SiO_2, and TiO_2 has previously been explored and documented.[33,37,48] In this work, TiO_2 was chosen as the ceramic additive following our earlier demonstration of its beneficial effects in PVdF-based polymer electrolytes.[31] A schematic of the composite polymer electrolyte depicting the role of the constituents is shown in Figure 2a. For material characterization, the viscous CPE blend was cast into circular disks and dried. Upon drying, the viscous blend becomes a thin, stand alone membrane that can be handled using a tweezer as shown in Figure 2b. Morphological characterization of the composite polymer electrolyte was carried out using SEM and EDS analyses. The SEM image of the dried CPE (Figure S1a, Supporting Information) shows the smooth nature of its top surface. Elemental maps (Figure S1b−f, Supporting Information) of the top surface show the uniform distribution of the constituent elements, namely, Mg, C, S, Ti, and Cl, indicating a uniform dispersion of the salt, ionic liquid, and the nanoparticles within the polymer composite. For electrochemical characterization of the CPE using Mg | Mg symmetric cells, the CPE blend was directly coated onto the Mg foil using a micrometer-adjustable film applicator and dried thereafter. Two 100 μm thick Mg foils were used for assembling the Mg | Mg symmetric cell. The surfaces of the foils were scraped with a stainless-steel blade to remove the inherent insulating oxide layer and expose the shiny Mg metal underneath. The thickness of the polymer layer was tuned to be within 60−80 μm, which is sufficient to ensure electrode separation and

DOI: 10.1021/acsaem.9b01455
ACS Appl. Energy Mater. 2019, 2, 7980−7990

be capable of achieving facile Mg-ion transport across the electrolyte (Figure S2a,b, Supporting Information).

Thermogravimetric analysis (TGA) was carried out to evaluate the thermal stability of the CPE and compare it with that of the pristine polymer (PVdF-HFP), and the magnesium salt ($Mg(ClO_4)_2$) (Figure S3, Supporting Information). The pristine PVdF-HFP shows a high thermal stability for up to 400 °C, after which a sudden loss of up to 60 wt % is observed until 480 °C. This weight loss can be attributed to C−H scission, followed by the formation of HF and the C═C bond.[43] The anhydrous $Mg(ClO_4)_2$ salt is known to undergo decomposition between 390 and 440 °C,[49] which was observed in our case as well. The initial weight loss of ∼10 wt % between 200 and 300 °C prior to this decomposition could be due to the loss of absorbed water molecules.[50] For the case of CPE, there is weight loss initiating at 90 °C. This ∼10% loss could be attributed to the removal of remnant solvent from the polymer mixture. From 200 to 300 °C, there is a continuous weight loss of up to 50 wt %, similar to the trends reported in PVdF−salt electrolyte blends.[33,43] Therefore, the CPE is thermally stable until at least 200 °C after which it undergoes degradation.

Measurement of the ionic conductivity is of paramount importance while characterizing polymer and inorganic solid-state electrolytes.[51] The ionic conductivity was measured through an electrochemical impedance spectroscopy (EIS) technique, wherein the polymer electrolyte was sandwiched between two stainless-steel blocking electrodes.[33,51] The room-temperature conductivity of the electrolyte was then calculated using the formula

$$\sigma = \frac{l}{R_b A} \tag{1}$$

where l and A denote the thickness and surface area of the electrolyte layer, respectively, and R_b denotes the bulk resistance (the x-intercept at the high-frequency region) obtained from the Nyquist plot.[52] The conductivity of the as-synthesized CPE was calculated to be 1.6×10^{-4} S cm^{-1} at 30 °C, a value that is close to the ionic conductivities of previously reported Mg polymer electrolytes.[33,34,48]

The activation energy of a polymer electrolyte represents the height of the energy barrier for ion migration and therefore serves as a measure of how energy-expensive it is for the ions to migrate within the polymer matrix.[48] The value of activation energy could be obtained by plotting the temperature dependence of the ionic conductivity. Figure 2c shows the Nyquist plots obtained at different temperatures for a cell assembled with two blocking electrodes. Figure 2d shows the temperature−conductivity traces obtained for three samples as follows: (i) CPE, i.e., the polymer composite sample containing the ionic liquid and TiO_2, (ii) $Mg(ClO_4)_2$−PVdF-HFP−IL, i.e., the polymer sample containing the ionic liquid, but without TiO_2, and (iii) $Mg(ClO_4)_2$−PVdF-HFP−TiO_2, i.e., the polymer composite sample containing TiO_2, but without the ionic liquid. The conductivities of the CPE are remarkably higher than those of the samples without either the ionic liquid or the TiO_2 nanoparticles at all temperatures. This shows the beneficial effect of having both the ionic liquid and the TiO_2 nanoparticles in the CPE. The temperature dependence curves of all three samples show a nonlinear behavior. Therefore, the curves have been fit with the Vogel−Tammann−Fulcher (VTF) equation given by

$$\sigma(T) = AT^{-0.5} \exp \frac{-E_a}{R(T - T_0)} \tag{2}$$

where A is a prefactor; E_a is a pseudoactivation energy; R is the gas constant; and T_0 is the Vogel temperature, which is related to the glass transition temperature ($T_0 = T_g - 50$ °C).[53,54] For PVdF-based electrolytes, T_0 is typically taken as 179 K.[33] The activation energy of the CPE was calculated to be 0.13 eV from the fit profile. The calculated value of activation energy is comparable to those of previously reported composite polymer electrolytes for both Li and Mg batteries.[30,48,55,56]

Another important parameter is the transport number, which quantifies the fraction of ionic transport and the cationic contribution to the conductivity of any metal-ion-conducting electrolyte. The transport number of the CPE was determined using the steady-state current method developed by Bruce and Vincent,[57] wherein the electrolyte is sandwiched between two nonblocking electrodes (Mg foils, in this case). A constant potential bias, ΔV, is applied to this setup, and the current, I, is obtained as a function of time. The current response of such a symmetric Mg | Mg cell under a constant potential bias of 0.05 V is shown in Figure 2f. AC impedance of this cell was measured both before and after the polarization experiment, and the Nyquist plots thus obtained are shown in Figure 2e. The values of the electrode−electrolyte interfacial resistances were obtained from these Nyquist plots. The cationic transport number t_+ was then obtained from the formula

$$t_+ = \frac{I_{ss}(\Delta V - I_0 R_{i,0})}{I_0(\Delta V - I_{ss} R_{i,ss})} \tag{3}$$

where I_0 and I_{ss} are the initial and steady-state currents, respectively, and $R_{i,0}$ and $R_{i,ss}$ are the initial and steady-state resistances of the interface, respectively.[58,59] The cationic transport number measured using this relation was found to be 0.23. This t_+ value is notably close to those of the existing polymer electrolytes that use liquid plasticizers.[33,34] The polarization experiment showing a flow of steady positive current in the Mg | Mg symmetric cell for a period of 1 h also serves as a confirmation for Mg-ion transport through the electrolyte. Although this method for computing the transport number was originally proposed for electrolytes containing univalent salts (such as Li^+ or Na^+), Balsara et al. noted in a separate analysis that this equation is in fact applicable to all binary salts, irrespective of the charge of the cation.[60] Therefore, the value of t_+ obtained here indeed denotes the transport number of Mg^{2+} cations in the electrolyte.

Additionally, the transport number could also be estimated using the solid-state pulsed-field gradient nuclear magnetic resonance (PFG-NMR) technique. This technique has been previously carried out successfully for estimating the transport number of Li^+ polymer electrolytes.[59] However, for the case of Mg, obtaining accurate spectra is notably difficult because of the low natural abundance of the ^{25}Mg isotope and sensitivity issues resulting from its quadrupolar nucleus.[61]

The ability of the polymer electrolyte to deposit Mg onto a substrate was verified through elemental analysis using energy-dispersive X-ray spectroscopy (EDS) and X-ray photoelectron spectroscopy (XPS). To deposit Mg onto a stainless-steel disc, a discharge current of 0.10 mA cm^{-2} was applied for 10 h onto a two-electrode Mg | stainless-steel setup, with the polymer electrolyte sandwiched between the electrodes. The Mg-deposited stainless-steel disc was then recovered and used

DOI: 10.1021/acsaem.9b01455
ACS Appl. Energy Mater. 2019, 2, 7980−7990

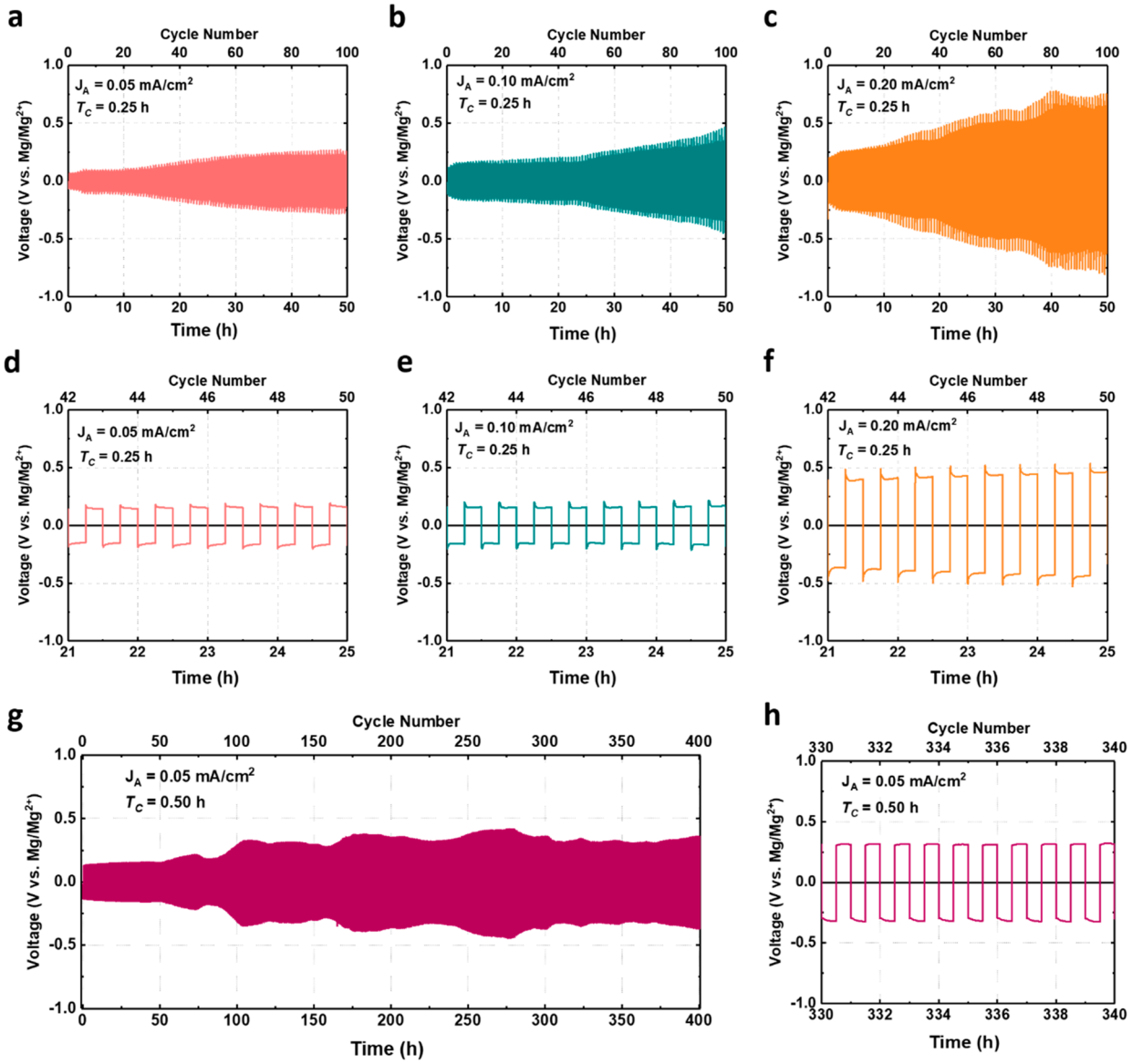

Figure 3. Galvanostatic cycling of two-electrode Mg | CPE | Mg cells carried out at current densities (J_A) of (a) 0.05 mA cm^{-2}, (b) 0.10 mA cm^{-2}, and (c) 0.20 mA cm^{-2} for a plating/stripping time of T_C = 0.25 h. Representative cycle numbers 42−50 of cycling tests carried out at current densities of (d) 0.05 mA cm^{-2}, (e) 0.10 mA cm^{-2}, and (f) 0.20 mA cm^{-2}. (g) Galvanostatic cycling carried out for a plating/stripping time of T_C = 0.50 h at a current density of 0.05 mA cm^{-2}. (h) Representative cycle numbers 330−340 of the cycling test carried out at T_C = 0.5 h.

for SEM, EDS, and XPS analyses. The SEM image (Figure S4a, Supporting Information) of the surface of a stainless-steel disc showed planar deposits, free of any dendritic growth. A uniform distribution of Mg was observed in the elemental map (Figure S4b, Supporting Information), confirming the elemental composition of the deposits on the stainless-steel disc. A sharp peak corresponding to the Mg 2p state was observed in the high-resolution XPS spectrum of the Mg deposit on the stainless-steel disc (Figure S4c, Supporting Information). However, the deconvolution of the XPS spectrum revealed the presence of additional peaks corresponding to MgO. This oxidation of the Mg deposits could have resulted from an exposure to the ambient atmosphere during sample transfer.

Ex situ SEM analysis of the CPE membrane taken from the cycled Mg | Mg cells was also carried out. The digital images of the CPE layer before and after cycling (Figures S5a and S5b, respectively, Supporting Information) show that the electrolyte did not undergo any significant structural change after cycling for 100 h. The minimal wear that is observed on the surface (Figure S5b) is the result of its strong adherence to the Mg foil within the cell. Comparison of the SEM images of the CPE before and after cycling (Figures S5c and S5d, respectively, Supporting Information) shows that the distribution of TiO_2 nanoparticles remains the same even after cycling for 100 h.

The magnesium deposition and stripping processes on the Mg electrode surface were confirmed through cyclic voltammetry (CV) performed using a symmetric two-electrode Mg | Mg cell (Figure S6a, Supporting Information). Occurrence of cathodic and anodic peaks denoting the deposition and stripping, respectively, could be clearly seen in the voltammogram. The CV plot resembles the ones obtained for Mg^{2+}-conducting polymer electrolytes developed by Kumar et al.[62] and by Pandey et al.[33] The decomposition voltage of the CPE was determined using a linear sweep voltammetry (LSV) test with an asymmetric Mg | SS two-

DOI: 10.1021/acsaem.9b01455
ACS Appl. Energy Mater. 2019, 2, 7980−7990

electrode cell within the voltage range of 1.0−5.0 V (Figure S6b, Supporting Information). The onset of a decomposition phenomenon begins at 3.1 V evidenced by the gradual increase in current. After 4.0 V, the current increases steeply, indicating the instability of the polymer electrolyte beyond this voltage. In contrast, the polymer electrolyte without the ionic liquid undergoes decomposition at a lower voltage of 2.4 V. This demonstrates the beneficial effect of the presence of the Pyr_{14}-TFSI ionic liquid in the CPE.

Although the occurrence of peaks in a cyclic voltammogram and a steady current in DC polarization test indicate Mg-ion transport in the electrolyte, galvanostatic cycling tests must be carried out to provide clear evidence of the reversible nature of the Mg plating/stripping from Mg-metal. The overpotential values observed in such galvanostatic cycling tests are a measure of the ease of Mg deposition/stripping from the Mg-metal surface and, therefore, help in determining the electrolyte's suitability in Mg-metal batteries. One of the earliest reports on Mg liquid electrolytes by Aurbach et al.[63] reported Mg dissolution/deposition overpotentials of 0.10 V for $Mg(AlCl_2EtBu)_2$/THF electrolyte at an applied current density of 0.5 mA cm^{-2}. More recently, Tutusaus et al.[64] reported overpotentials of 0.12 V at 0.1 mA cm^{-2} for the state-of-the-art liquid electrolyte $[Mg(CB_{11}H_{12})_2]$/tetraglyme developed by Toyota. Son et al.[65] reported galvanostatic cycling results with overpotentials of up to 0.10−0.30 V at 0.01 mA cm^{-2} to assert the favorable nature of their artificial interphase in Mg | $Mg(TFSI)_2$ | Mg cells. Such high overpotentials in the range of hundreds of millivolts are in sharp contrast to the few-mV overpotentials commonly observed in the case of Li metal.[66] This can be attributed to the significantly stronger cation−solvent and ion−ion interactions in divalent-metal ions compared to monovalent Li^+ ions.[67]

Although there have been several reports of Mg^{2+}-conducting polymer electrolytes, there is little evidence for their reversible plating/stripping with Mg-metal anodes at room temperature. To find out if our composite polymer electrolyte is capable of cycling, galvanostatic cycling tests were carried out with symmetric Mg | Mg two-electrode cells at different current densities, and their overpotentials were observed. Figure 3a−c shows the overpotential vs time plots of the Mg | Mg cells carried out at areal current densities (J_A) of 0.05, 0.10, and 0.20 mA cm^{-2}, respectively. The plating/stripping time (T_C) for each cycle was set to 0.25 h. For low and moderate current densities of 0.05 and 0.10 mA cm^{-2}, respectively, the deposition/stripping overpotentials were observed to be ≤0.15 V for the first 50 cycles. It must be noted that this value is comparable to the overpotential values of 0.12 V obtained with the most recent state-of-the-art liquid electrolyte, magnesium monocarborane $[Mg(CB_{11}H_{12})_2]$/tetraglyme.[64] At the end of 100 cycles, the deposition overpotential gradually increased to 0.23 V for the case of 0.05 mA cm^{-2} and to 0.31 V for the case of 0.10 mA cm^{-2}. However, for the cycling test carried out with a high current density of 0.20 mA cm^{-2}, a relatively higher overpotential was observed (Figure 3c). Toward the end of 50 cycles with 0.20 mA cm^{-2}, the overpotential stabilized to a value of 0.39 V. From then on, a gradual increase to 0.65 V was observed at the end of 100 cycles. Figure 3d−f shows the representative cycle numbers 42−50 of the cycling tests carried out at current densities of 0.05 mA cm^{-2}, 0.10 mA cm^{-2}, and 0.20 mA cm^{-2}, respectively. Flat voltage profiles, indicative of a smooth Mg plating/stripping process on the surface of Mg-metal, could be clearly seen in all three cases. To explore the effect of longer plating/stripping times, a symmetric Mg | Mg cell was cycled at 0.05 mA cm^{-2} with the plating/stripping time set to 0.50 h. Figure 3g shows the latter cycling results, where it could be seen that the deposition overpotential remains low at 0.20 V for up to 80 cycles, despite the longer plating/stripping process. Thereafter, a slight increase was observed, and the overpotential remained stable at ∼0.30 V for up to 400 cycles. The representative cycle numbers 330−340 shown in Figure 3h illustrate a voltage profile similar to that of earlier tests with flat plating/stripping features. Such a high degree of cycling reversibility for up to several hundred cycles is unique among the existing Mg-ion-conducting polymer electrolytes. Galvanostatic cycling tests were also carried out with a longer plating/stripping time of 1.0 h (Figure S7a,b, Supporting Information). The overpotential values were slightly higher than those of the tests done with 0.5 h, which could be a consequence of the increased amount of metal that needs to be stripped from the electrodes.

To understand the high performance of the CPE, the chemical environments of the Mg^{2+} ions and the polymer chains in the CPE were analyzed through Raman spectroscopy. Raman spectra were obtained at different stages of the synthesis to observe the effects of progressive addition of the precursors. Figure 4a shows the Raman spectra of the (i) pristine polymer (PVdF-HFP), (ii) $Mg(ClO_4)_2$/ionic liquid (I.L) mixture, (iii) $Mg(ClO_4)_2$/PVdF-HFP blend, (iv) $Mg(ClO_4)_2$/PVdF-HFP/I.L blend, and, the final CPE composition, (v) $Mg(ClO_4)_2$/PVdF-HFP/I.L/TiO_2 nanoparticles. Normalized intensities were used to compare and quantify the presence of constituent ions and functional groups at different stages during the synthesis. It is widely accepted that an ample dissociation of the salt into its cations and anions is essential to obtain high cationic conductivity in polymer electrolytes. Raman spectra in the region 800−1100 cm^{-1} in Figure 4a clearly show the gradual increase in the intensity of the peak at 937 cm^{-1} which corresponds to the ν_1 mode of vibration in the $(ClO_4)^-$ ion. This indicates a progressive increase in $(ClO_4)^-$ ions which could have resulted only due to the increased dissociation of the $Mg(ClO_4)_2$ salt into $(ClO_4)^-$ and Mg^{2+} ions. Therefore, the addition of ceramic fillers seems to have further improved the salt dissociation in the electrolyte (which is discussed in more detail in Figure 5).

Being highly charge dense, Mg^{2+} ions tend to strongly interact with $TFSI^-$ anions to form bulky coordination complexes.[46] Prior reports on ionic-liquid electrolytes synthesized using Mg salt and Pyr_{14}-TFSI ionic liquid have shown a coordination between Mg^{2+} and $TFSI^-$ ions.[46,47] To know if this interaction is present in the case of our composite polymer electrolyte, the Raman spectra in the region 700−800 cm^{-1} (Figure 4b) were analyzed. The peak at 742 cm^{-1} corresponds to the $TFSI^-$ expansion−contraction normal mode of vibration and denotes the "free" $TFSI^-$ anions that are not coordinated to Mg^{2+} cations.[47] The interaction between Mg^{2+} and $TFSI^-$ ions would be typically indicated by the origin of peaks at 746 and 752 cm^{-1} corresponding to their coordination in bridging and bidentate geometries, respectively.[47] However, in the case of our composite polymer, this characteristic peak did not show any new shoulders originating at higher wavenumbers upon addition of the ionic liquid. We believe that their coordination between Mg^{2+} and $TFSI^-$ ions (as seen in ionic-liquid electrolytes) might have been prevented by the presence of polymer chains and TiO_2 nanoparticles (also discussed in

DOI: 10.1021/acsaem.9b01455
ACS Appl. Energy Mater. 2019, 2, 7980−7990

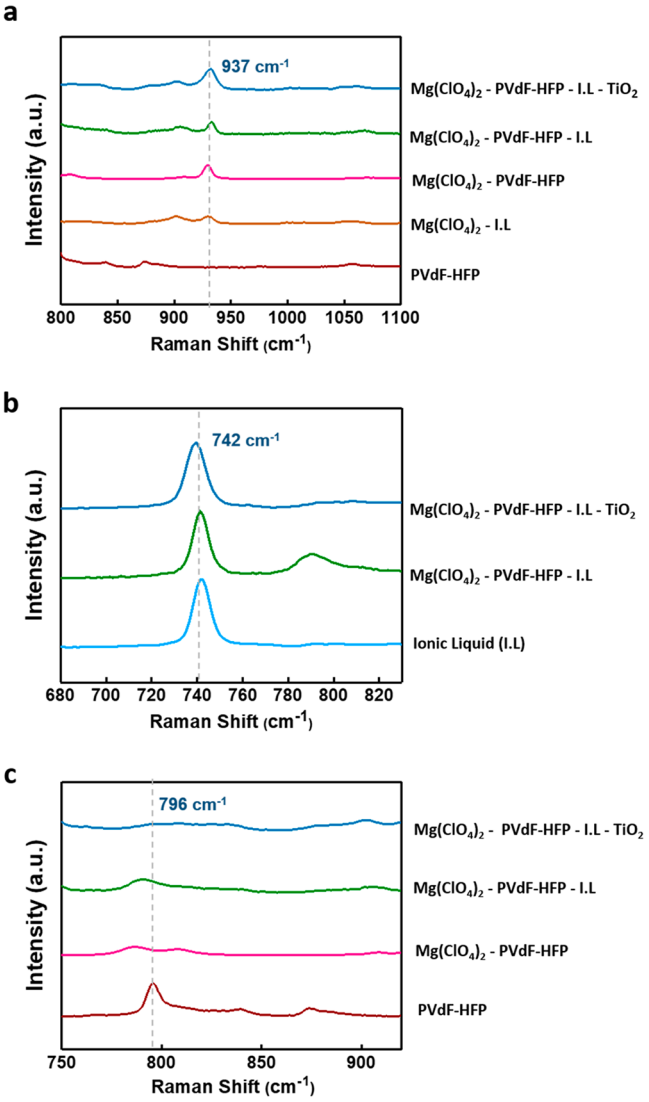

Figure 4. Comparison of Raman spectra of the CPE and different combinations of constituents in electrolytes in the regions (a) 800–1100 cm^{-1}, (b) 680–830 cm^{-1}, and (c) 750–920 cm^{-1}.

Figure 5d). Figure 4c shows the comparison of the Raman spectra in the region of the pristine polymer and the final composite. The peak at 796 cm^{-1}, corresponding to the crystalline phase (α-phase) of the PVdF,[68,69] gradually decreases upon addition of Mg salt and almost disappears in the final composite indicating the favorable loss of crystallinity of the polymer upon the addition of the salt and ionic liquid.

We also carried out classical molecular dynamics simulations to fully understand the migration behavior of Mg^{2+} ions in the polymer electrolyte (Figure 5a). Mean square displacement calculations demonstrate that the addition of ionic liquid significantly enhances the mobility of Mg^{2+} ions in PVdF from almost no ion mobility. Figure 5b shows that the addition of ceramic fillers, which can adsorb free $(ClO_4)^-$ ions, also increases the diffusivity of Mg^{2+} ions from 3.5×10^{-10} to 1.0×10^{-9} cm^2 s^{-1}. Such an increase of ion mobility is also supported by the calculated radial distribution functions (RDFs) (Figure 5c), which indicate that ceramic fillers lead to stronger electrostatic interaction between Mg^{2+} ions and F atoms of PVdF chains (larger and sharper peaks in RDFs) and further facilitate the mobility of Mg^{2+} ions through inter- and intramolecular PVdF chains. These computational results are in good agreement with Raman spectra analysis, confirming the role of both ionic liquid and ceramic fillers in improving the mobility of Mg^{2+} ions. Evaluated RDF calculations of Mg-TFSI ion pairs in Figure 5d show a decrease of the RDF peak of around 2 Å, confirming a weak coordination between $TFSI^-$ and Mg^{2+} ions as observed in the Raman spectra (Figure 4b).

These results suggest that a favorable Mg-ion transport within the polymer and deposition onto the electrode as observed could be explained by the combination of the following factors: (1) increased dissociation of salt into its constituent cations and anions, (2) absence of any significant coordination between Mg^{2+} ions of the salt and $TFSI^-$ ions of the ionic liquid, and (3) amorphization of the polymer upon addition of Mg salt and TiO_2 fillers. Further optimization of these constituents and a systematic investigation into specific interactions between the ionic species and polymer can aid in extending this technique to other magnesium salts and polymer candidates.

CONCLUSION

In summary, a composite polymer electrolyte (CPE) has been developed for application in room-temperature all-solid-state rechargeable magnesium batteries. Galvanostatic cycling with symmetric cells shows that this polymer electrolyte supports excellent cyclability with Mg-metal. For cycling tests carried out at current densities of 0.05 and 0.10 mA cm^{-2}, low deposition/stripping overpotentials of 0.3 V for up to 400 cycles and of 0.2 V for up to 80 cycles, respectively, were observed. Interestingly, these solid-state Mg-deposition overpotential values are similar to those obtained for the present state-of-the-art liquid Mg electrolytes. Raman spectra analysis indicated an increased dissociation of the precursor salt upon the addition of ionic liquid and ceramic fillers. Furthermore, no significant interaction was observed between the $TFSI^-$ anions of the ionic liquid and Mg^{2+} cations, which would otherwise impede the motion of Mg^{2+} ions across the polymer. An optimization of the composition and further investigation into the deposition mechanism are necessary to understand the increasing overpotential values for high current densities (0.20 mA cm^{-2}). Nevertheless, we believe that the development of this composite polymer electrolyte is a significant step toward enabling highly cyclable room-temperature solid-state magnesium batteries.

EXPERIMENTAL SECTION

Synthesis of the Composite Polymer Electrolyte (CPE). An amount of 1.1 g of magnesium perchlorate ($Mg(ClO_4)_2$, Sigma-Aldrich, Inc.) was dissolved in 3 mL of acetone. The ratio of the following constituents is expressed as weight percentage (wt %) with respect to $Mg(ClO_4)_2$. In a separate vial, 30 wt % of poly(vinylidene fluoride-*co*-hexafluoropropylene) (PVdF-HFP) pellets (Sigma-Aldrich, Inc.) were dissolved in a few mL of acetone at 40 °C and added to the $Mg(ClO_4)_2$ solution. To this mixture, 75 wt % of ionic liquid, 1-butyl-1-methylpyrrolidinium bis(trifluoromethyl)sulfonyl imide (Pyr_{14}-TFSI, Iolitec Ltd.), was added and stirred well. This was followed by the addition of 10 wt % of TiO_2 nanoparticle powder (US Research Nanomaterials, Inc.). This mixture was stirred in a magnetic stirrer at 60 °C for 12 h to get a white, viscous CPE blend. Prior to the synthesis, $Mg(ClO_4)_2$, PVdF-HFP, and Pyr_{14}-TFSI were dried in a vacuum for 12 h. TiO_2 nanoparticles were annealed at 150 °C in a vacuum for 24 h to remove any surface-adsorbed moisture.

Casting. Circular Mg disks of 15 mm diameter each were punched from magnesium foil (0.1 mm thick, MTI Corporation). The polymer

DOI: 10.1021/acsaem.9b01455
ACS Appl. Energy Mater. 2019, 2, 7980–7990

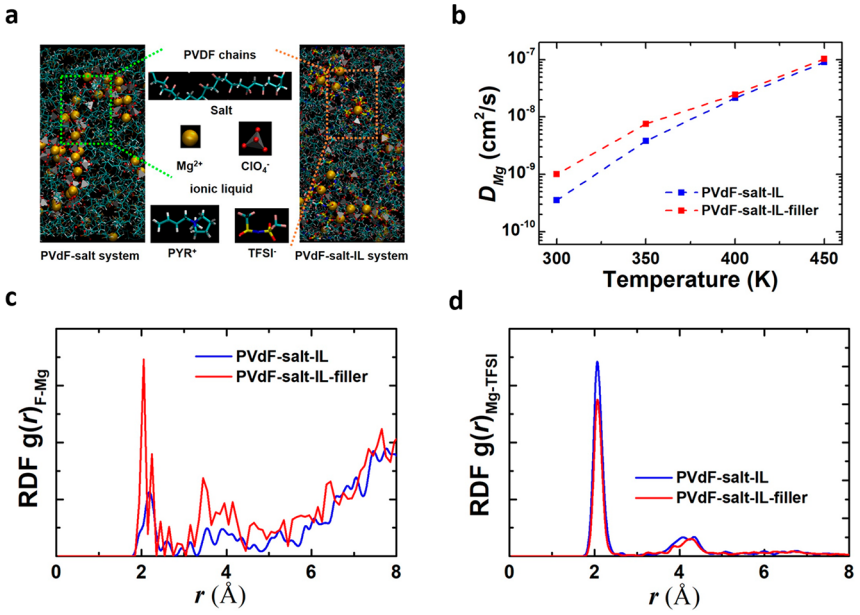

Figure 5. Classical molecular dynamics simulations of Mg^{2+} migration in the CPE. (a) Schematic of simulation models of PVdF−salt systems with and without ionic liquids. (b) Predicted diffusivities of Mg^{2+} ions D_{Mg} in the polymer electrolyte at different temperatures. (c,d) Radial distribution functions (RDFs) of Mg-F (c) and Mg-TFSI pairs (d) in the polymer electrolyte with and without considering ceramic fillers.

was cast onto these circular Mg disks using a micrometer-adjustable film applicator. Prior to coating, the oxide layer on the Mg disk surface was scraped off using a blade until the shiny Mg-metal layer was revealed. The thickness of the polymer melt was adjusted to be within 60−80 μm. The casting was dried at 80 °C.

Morphological, Structural, and Thermal Characterization. The surface morphologies and elemental maps of the polymer sample and the cross-section of Mg foil | CPE were examined through scanning electron microscopy (Hitachi VPSEM S-3000N) linked with energy-dispersive X-ray analysis. Raman spectra of all the samples were obtained using a confocal Raman microscope (Renishaw InVia Reflex) employing a green 532 nm/50 mW diode pumped solid state laser. Thermal stabilities of the samples were analyzed using a TA Instruments model Q5000IR thermogravimetric analyzer (TGA).

Symmetric Cell Setup. A fresh Mg foil was placed on top of the dried polymer | Mg disk to make a Mg | Mg symmetric cell setup. This two-electrode cell setup was used for carrying out electrochemical characterization and galvanostatic cycling tests.

Electrochemical Characterization. Galvanostatic charge/discharge cycling, electrochemical impedance spectroscopy (EIS), DC polarization, and cyclic voltammetry experiments were performed using a Bio-Logic VMP3 multichannel potentiostat/galvanostat equipped with EC-Lab software. The polymer electrolyte was sandwiched between two stainless-steel discs which acted as blocking electrodes. The AC impedance spectra were measured in the frequency range of 200 kHz to 50 mHz. DC polarization on the Mg | Mg symmetric cell was carried out at a constant step voltage of 0.1 V. CV experiments were performed using a Mg | Mg symmetric cell at a sweep rate of 10 mV s^{-1}. Galvanostatic cycling of Mg | Mg symmetric cells was carried out at areal current densities of 0.05, 0.10, and 0.20 mA cm^{-2} for two different plating/stripping times of 0.25 and 0.50 h.

Classical Molecular Dynamics Simulations. All our molecular dynamics simulations were carried out using the parallelized LAMMPS package.[70] The force fields developed by Chaban[71] and Lopes et al.[72] as well as Lachet et al.[73] were utilized to describe both intramolecular and intermolecular interaction of ionic liquids Pyr_{14}-TFSI and PVdF, respectively. A recently developed Lennard-Jones potential[74] was used to describe interaction of Mg-salt $Mg(ClO_4)_2$. Cross-term interaction among the ionic liquid, PVdF, and Mg salt was described by the Lorentz−Berthelot rule. All the force field parameters are given in Tables S1−3 (Supporting Information). A mixture of 30 PVdF molecule chains (80 CF_2 monomers), 60 $Mg(ClO_4)_2$, and 120 Pyr_{14}-TFSI molecules was constructed to simulate a model of polymer electrolyte with ionic liquids. The model of solid electrolyte without ionic liquids was considered as well. To take into account the adsorption of ClO_4^- anions by TiO_2 nanoparticles, a noncharge neutral model was constructed by removing ClO_4^- anions until the ratio $N(Mg^{2+}):N(ClO_4^-)$ equals 2:1. A melt-and-quench procedure[75,76] was utilized to relax all amorphous models to their steady-state mixed states at different temperatures. Since the migration of Mg^{2+} ions is too slow at room temperature (300 K), which requires extremely long simulation time, all the simulation models were run under NPT ensemble at temperatures of 350, 400, and 450 K to accelerate the Mg^{2+} transport. Mean square displacements (MSDs) of Mg^{2+} ions as a function of simulation time were calculated according to the equation

$$\mathrm{MSD} = \left\langle \sum_{i=1}^{3} |r_i(t) - r_i(0)|^2 \right\rangle = \frac{1}{N} \sum_{j=1}^{N} \sum_{i=1}^{3} |r_i^j(t) - r_i^j(0)|^2$$

where N is the total atom number; $\langle K \rangle$ denotes the average value over all atoms; and $r_i(0)$ and $r_i(t)$ are i-axis positions at simulation time 0 and t. Einstein's relation MSD = $6Dt$ was then utilized to calculate the diffusivity of Mg^{2+} ions D_{Mg} at the corresponding temperature. Finally, the Arrhenius relation $D_T = D_0 \exp\left(-\frac{E_{ba}}{k_b T}\right)$ was used to extrapolate the value of D_{Mg} at room temperature, E_{ba}, k_B, T, and D_0 being the energy barrier, the Boltzmann constant, temperature, and the prefactor. Radial distribution functions (RDFs) were evaluated to analyze the atomic structures of polymer electrolyte models.

■ ASSOCIATED CONTENT

Supporting Information

The Supporting Information is available free of charge on the ACS Publications website at DOI: 10.1021/acsaem.9b01455.

SEM images and thermogravimetric analysis of the composite polymer electrolyte (CPE), ex situ SEM and XPS analysis of the Mg-deposited stainless-steel electrode, cyclic voltammogram of a Mg | Mg cell, linear sweep voltammogram of a Mg | stainless-steel cell,

DOI: 10.1021/acsaem.9b01455
ACS Appl. Energy Mater. 2019, 2, 7980−7990

and force field parameters of the molecular dynamics simulations (PDF)

AUTHOR INFORMATION

Corresponding Author

*E-mail: rsyassar@uic.edu.

ORCID

Ramasubramonian Deivanayagam: 0000-0003-1367-009X
Tara Foroozan: 0000-0003-1334-3048
Nikhil V. Medhekar: 0000-0003-3124-4430
Reza Shahbazian-Yassar: 0000-0002-7744-4780

Notes

The authors declare no competing financial interest.

ACKNOWLEDGMENTS

R. Shahbazian-Yassar acknowledges the financial support from the National Science Foundation (NSF) CBET award no. 1805938. R. Deivanayagam's efforts were supported by NSF DMR award no. 1620901. We are thankful to the Battery Technology Laboratory of the College of Engineering at the University of Illinois at Chicago (UIC). This work made use of instruments in the Electron Microscopy Service (Research Resources Center) and the Nanotechnology Core Facility (NCF) at UIC. M. Wang, V. Vasudevan, and N. V. Medhekar acknowledge support from the Monash University Cluster, the Australian National Computing Infrastructure (NCI), and the Pawsey Supercomputing Center for high performance computing. N. V. Medhekar gratefully acknowledges the financial support from the Australian Research Council's Discovery Project Scheme (DP160103661).

REFERENCES

(1) Muldoon, J.; Bucur, C. B.; Gregory, T. Quest for Nonaqueous Multivalent Secondary Batteries: Magnesium and Beyond. *Chem. Rev.* **2014**, *114*, 11683−11720.

(2) Xu, C.; Chen, Y.; Shi, S.; Li, J.; Kang, F.; Su, D. Secondary Batteries with Multivalent Ions for Energy Storage. *Sci. Rep.* **2015**, *5*, 14120.

(3) Wang, R. Y.; Shyam, B.; Stone, K. H.; Weker, J. N.; Pasta, M.; Lee, H. W.; Toney, M. F.; Cui, Y. Reversible Multivalent (Monovalent, Divalent, Trivalent) Ion Insertion in Open Framework Materials. *Adv. Energy Mater.* **2015**, *5*, 1401869.

(4) Lin, M. C.; Gong, M.; Lu, B.; Wu, Y.; Wang, D.-Y.; Guan, M.; Angell, M.; Chen, C.; Yang, J.; Hwang, B. J.; Dai, H. An Ultrafast Rechargeable Aluminium-Ion Battery. *Nature* **2015**, *520* (7547), 324−328.

(5) Li, H.; Han, C.; Huang, Y.; Huang, Y.; Zhu, M.; Pei, Z.; Xue, Q.; Wang, Z.; Liu, Z.; Tang, Z.; Wang, Y.; Kang, F.; Li, B.; Zhi, C. An Extremely Safe and Wearable Solid-State Zinc Ion Battery Based on a Hierarchical Structured Polymer Electrolyte. *Energy Environ. Sci.* **2018**, *11* (4), 941−951.

(6) Gummow, R. J.; Vamvounis, G.; Kannan, M. B.; He, Y. Calcium-Ion Batteries: Current State-of-the-Art and Future Perspectives. *Adv. Mater.* **2018**, *30*, 1801702.

(7) Das, S. K.; Mahapatra, S.; Lahan, H. Aluminium-Ion Batteries: Developments and Challenges. *J. Mater. Chem. A* **2017**, *5* (14), 6347−6367.

(8) Saha, P.; Datta, M. K.; Velikokhatnyi, O. I.; Manivannan, A.; Alman, D.; Kumta, P. N. Rechargeable Magnesium Battery: Current Status and Key Challenges for the Future. *Prog. Mater. Sci.* **2014**, *66*, 1−86.

(9) Yoo, H. D.; Shterenberg, I.; Gofer, Y.; Gershinsky, G.; Pour, N.; Aurbach, D. Mg Rechargeable Batteries: An on-Going Challenge. *Energy Environ. Sci.* **2013**, *6* (8), 2265−2279.

(10) Bucur, C. B.; Gregory, T.; Oliver, A. G.; Muldoon, J. Confession of a Magnesium Battery. *J. Phys. Chem. Lett.* **2015**, *6* (18), 3578−3591.

(11) Mohtadi, R.; Mizuno, F. Magnesium Batteries: Current State of the Art, Issues and Future Perspectives. *Beilstein J. Nanotechnol.* **2014**, *5* (1), 1291−1311.

(12) Deivanayagam, R.; Ingram, B. J.; Shahbazian-Yassar, R. Progress in Development of Electrolytes for Magnesium Batteries. *Energy Storage Mater.* **2019**, *21*, 136−153.

(13) Song, J.; Sahadeo, E.; Noked, M.; Lee, S. B. Mapping the Challenges of Magnesium Battery. *J. Phys. Chem. Lett.* **2016**, *7* (9), 1736−1749.

(14) Choi, J. W.; Aurbach, D. Promise and Reality of Post-Lithium-Ion Batteries with High Energy Densities. *Nat. Rev. Mater.* **2016**, *1* (4), 16013.

(15) Aurbach, D.; Gizbar, H.; Schechter, A.; Chusid, O.; Gottlieb, H. E.; Gofer, Y.; Goldberg, I. Electrolyte Solutions for Rechargeable Magnesium Batteries Based on Organomagnesium Chloroaluminate Complexes. *J. Electrochem. Soc.* **2002**, *149* (2), A115.

(16) Duffort, V.; Sun, X.; Nazar, L. F. Screening for Positive Electrodes for Magnesium Batteries: A Protocol for Studies at Elevated Temperatures. *Chem. Commun.* **2016**, *52* (84), 12458−12461.

(17) Canepa, P.; Sai Gautam, G.; Hannah, D. C.; Malik, R.; Liu, M.; Gallagher, K. G.; Persson, K. A.; Ceder, G. Odyssey of Multivalent Cathode Materials: Open Questions and Future Challenges. *Chem. Rev.* **2017**, *117*, 4287−4341.

(18) Kim, S. U.; Perdue, B.; Apblett, C. A.; Srinivasan, V. Understanding Performance Limitations to Enable High Performance Magnesium-Ion Batteries. *J. Electrochem. Soc.* **2016**, *163* (8), A1535−A1542.

(19) Liebenow, C. Reversibility of Electrochemical Magnesium Deposition from Grignard Solutions. *J. Appl. Electrochem.* **1997**, *27* (2), 221−225.

(20) Aurbach, D.; Weissman, I.; Gofer, Y.; Levi, E. Nonaqueous Magnesium Electrochemistry and Its Application in Secondary Batteries. *Chem. Rec.* **2003**, *3* (1), 61−73.

(21) Mizrahi, O.; Amir, N.; Pollak, E.; Chusid, O.; Marks, V.; Gottlieb, H.; Larush, L.; Zinigrad, E.; Aurbach, D. Electrolyte Solutions with a Wide Electrochemical Window for Rechargeable Magnesium Batteries. *J. Electrochem. Soc.* **2008**, *155* (2), A103−A109.

(22) Nelson, E. G.; Brody, S. I.; Kampf, J. W.; Bartlett, B. M. A Magnesium Tetraphenylaluminate Battery Electrolyte Exhibits a Wide Electrochemical Potential Window and Reduces Stainless Steel Corrosion. *J. Mater. Chem. A* **2014**, *2* (43), 18194−18198.

(23) Meyer, W. H. Polymer Electrolytes for Lithium-Ion Batteries. *Adv. Mater.* **1998**, *10* (6), 439−448.

(24) Xue, Z.; He, D.; Xie, X. Poly(Ethylene Oxide)-Based Electrolytes for Lithium-Ion Batteries. *J. Mater. Chem. A* **2015**, *3* (38), 19218−19253.

(25) Capuano, F.; Croce, F.; Scrosati, B. Composite Polymer Electrolytes. *J. Electrochem. Soc.* **1991**, *138* (7), 1918−1922.

(26) Porcarelli, L.; Gerbaldi, C.; Bella, F.; Nair, J. R. Super Soft All-Ethylene Oxide Polymer Electrolyte for Safe All-Solid Lithium Batteries. *Sci. Rep.* **2016**, *6* (1), 19892.

(27) Weston, J. E.; Steele, B. C. H. Effects of Inert Fillers on the Mechanical and Electrochemical Properties of Lithium Salt-Poly-(Ethylene Oxide) Polymer Electrolytes. *Solid State Ionics* **1982**, *7* (1), 75−79.

(28) Croce, F.; Appetecchi, G. B.; Persi, L.; Scrosati, B. Nanocomposite Polymer Electrolytes for Lithium Batteries. *Nature* **1998**, *394* (6692), 456−458.

(29) Croce, F.; Persi, L. L.; Scrosati, B.; Serraino-Fiory, F.; Plichta, E.; Hendrickson, M. A. Role of the Ceramic Fillers in Enhancing the Transport Properties of Composite Polymer Electrolytes. *Electrochim. Acta* **2001**, *46* (16), 2457−2461.

(30) Song, S.; Yang, S.; Zheng, F.; Zeng, K.; Duong, H. M.; Savilov, S. V.; Aldoshin, S. M.; Hu, N.; Lu, L. Communication—Poly-(Ethylene Oxide)-Immobilized Ionogel with High Ionic Liquid

DOI: 10.1021/acsaem.9b01455
ACS Appl. Energy Mater. 2019, 2, 7980−7990

Loading and Superior Ionic Conductivity. *J. Electrochem. Soc.* **2016**, *163* (14), A2887−A2889.
(31) Cheng, M.; Jiang, Y.; Yao, W.; Yuan, Y.; Deivanayagam, R.; Foroozan, T.; Huang, Z.; Song, B.; Rojaee, R.; Shokuhfar, T.; Pan, Y.; Lu, J.; Shahbazian-Yassar, R. Elevated-Temperature 3D Printing of Hybrid Solid-State Electrolyte for Li-Ion Batteries. *Adv. Mater.* **2018**, *30* (39), 1800615.
(32) Chusid, O.; Gofer, Y.; Gizbar, H.; Vestfrid, Y.; Levi, E.; Aurbach, D.; Riech, I. Solid-State Rechargeable Magnesium Batteries. *Adv. Mater.* **2003**, *15* (7), 627−630.
(33) Pandey, G. P.; Agrawal, R. C.; Hashmi, S. A. Magnesium Ion-Conducting Gel Polymer Electrolytes Dispersed with Nanosized Magnesium Oxide. *J. Power Sources* **2009**, *190* (2), 563−572.
(34) Pandey, G. P.; Hashmi, S. A. Experimental Investigations of an Ionic-Liquid-Based, Magnesium Ion Conducting, Polymer Gel Electrolyte. *J. Power Sources* **2009**, *187* (2), 627−634.
(35) Kumar, Y.; Hashmi, S. A.; Pandey, G. P. Ionic Liquid Mediated Magnesium Ion Conduction in Poly(Ethylene Oxide) Based Polymer Electrolyte. *Electrochim. Acta* **2011**, *56* (11), 3864−3873.
(36) Pandey, G. P.; Agrawal, R. C.; Hashmi, S. A. Performance Studies on Composite Gel Polymer Electrolytes for Rechargeable Magnesium Battery Application. *J. Phys. Chem. Solids* **2011**, *72* (12), 1408−1413.
(37) Shao, Y.; Rajput, N. N.; Hu, J.; Hu, M.; Liu, T.; Wei, Z.; Gu, M.; Deng, X.; Xu, S.; Han, K. S.; Wang, J.; Nie, Z.; Li, G.; Zavadil, K. R.; Xiao, J.; Wang, C.; Henderson, W. A.; Zhang, J.-G.; Wang, Y.; Mueller, K. T.; Persson, K.; Liu, J. Nanocomposite Polymer Electrolyte for Rechargeable Magnesium Batteries. *Nano Energy* **2015**, *12*, 750−759.
(38) Ponmani, S.; Ramesh Prabhu, M. Sulfonate Based Ionic Liquid Incorporated Polymer Electrolytes for Magnesium Secondary Battery. *Polym. - Plast. Technol. Eng.* **2019**, *58* (9), 978−991.
(39) Oh, J. S.; Ko, J. M.; Kim, D. W. Preparation and Characterization of Gel Polymer Electrolytes for Solid State Magnesium Batteries. *Electrochim. Acta* **2004**, *50*, 903−906.
(40) Pandey, G. P.; Agrawal, R. C.; Hashmi, S. A. Magnesium Ion-Conducting Gel Polymer Electrolytes Dispersed with Fumed Silica for Rechargeable Magnesium Battery Application. *J. Solid State Electrochem.* **2011**, *15* (10), 2253−2264.
(41) Tripathi, S. K.; Jain, A.; Gupta, A.; Mishra, M. Electrical and Electrochemical Studies on Magnesium Ion-Based Polymer Gel Electrolytes. *J. Solid State Electrochem.* **2012**, *16* (5), 1799−1806.
(42) Du Pasquier, A.; Warren, P. C.; Culver, D.; Gozdz, A. S.; Amatucci, G. G.; Tarascon, J. M. Plastic PVDF-HFP Electrolyte Laminates Prepared by a Phase-Inversion Process. *Solid State Ionics* **2000**, *135* (1−4), 249−257.
(43) Kotobuki, M.; Lu, L.; Savilov, S. V.; Aldoshin, S. M. Poly(Vinylidene Fluoride)-Based Al Ion Conductive Solid Polymer Electrolyte for Al Battery. *J. Electrochem. Soc.* **2017**, *164* (14), A3868−A3875.
(44) Osada, I.; De Vries, H.; Scrosati, B.; Passerini, S. Ionic-Liquid-Based Polymer Electrolytes for Battery Applications. *Angew. Chem., Int. Ed.* **2016**, *55* (2), 500−513.
(45) Ye, Y. S.; Rick, J.; Hwang, B. J. Ionic Liquid Polymer Electrolytes. *J. Mater. Chem. A* **2013**, *1* (8), 2719−2743.
(46) Giffin, G. A.; Moretti, A.; Jeong, S.; Passerini, S. Complex Nature of Ionic Coordination in Magnesium Ionic Liquid- Based Electrolytes: Solvates with Mobile Mg 2+ Cations. *J. Phys. Chem. C* **2014**, *118*, 9966−9973.
(47) Jeremias, S.; Giffin, G. A.; Moretti, A.; Jeong, S.; Passerini, S. Mechanisms of Magnesium Ion Transport in Pyrrolidinium Bis-(Trifluoromethanesulfonyl)Imide-Based Ionic Liquid Electrolytes. *J. Phys. Chem. C* **2014**, *118* (49), 28361−28368.
(48) Song, S.; Kotobuki, M.; Zheng, F.; Li, Q.; Xu, C.; Wang, Y.; Li, W. D. Z.; Hu, N.; Lu, L. Communication—A Composite Polymer Electrolyte for Safer Mg Batteries. *J. Electrochem. Soc.* **2017**, *164* (4), A741−A743.
(49) Acheson, R. J.; Jacobs, P. W. M. The Thermal Decomposition of Magnesium Perchlorate and of Ammonium Perchlorate and Magnesium Perchlorate Mixtures. *J. Phys. Chem.* **1970**, *74* (2), 281−288.
(50) Robertson, K.; Bish, D. Determination of the Crystal Structure of Magnesium Perchlorate Hydrates by X-Ray Powder Diffraction and the Charge-Flipping Method. *Acta Crystallogr., Sect. B: Struct. Sci.* **2010**, *66* (6), 579−584.
(51) Uddin, M.-J.; Cho, S.-J. Reassessing the Bulk Ionic Conductivity of Solid-State Electrolytes. *Sustain. Energy Fuels* **2018**, *2* (7), 1458−1462.
(52) Qian, X.; Gu, N.; Cheng, Z.; Yang, X.; Wang, E.; Dong, S. Methods to Study the Ionic Conductivity of Polymeric Electrolytes Using a.c. Impedance Spectroscopy. *J. Solid State Electrochem.* **2001**, *6* (1), 8−15.
(53) Chintapalli, M.; Le, T. N. P.; Venkatesan, N. R.; Mackay, N. G.; Rojas, A. A.; Thelen, J. L.; Chen, X. C.; Devaux, D.; Balsara, N. P. Structure and Ionic Conductivity of Polystyrene- Block -Poly-(Ethylene Oxide) Electrolytes in the High Salt Concentration Limit. *Macromolecules* **2016**, *49*, 1770−1780.
(54) Diederichsen, K. M.; Buss, H. G.; McCloskey, B. D. The Compensation Effect in the Vogel-Tammann-Fulcher (VTF) Equation for Polymer-Based Electrolytes. *Macromolecules* **2017**, *50* (10), 3831−3840.
(55) Liu, W.; Lee, S. W.; Lin, D.; Shi, F.; Wang, S.; Sendek, A. D.; Cui, Y. Enhancing Ionic Conductivity in Composite Polymer Electrolytes with Well-Aligned Ceramic Nanowires. *Nat. Energy* **2017**, *2* (5), 17035.
(56) Liu, W.; Liu, N.; Sun, J.; Hsu, P.; Li, Y.; Lee, H.; Cui, Y. Ionic Conductivity Enhancement of Polymer Electrolytes with Ceramic Nanowire Fillers. *Nano Lett.* **2015**, *15*, 2740−2745.
(57) Evans, J.; Vincent, C. A.; Bruce, P. G. Electrochemical Measurement of Transference Numbers in Polymer Electrolytes. *Polymer* **1987**, *28* (13), 2324−2328.
(58) Chintapalli, M.; Timachova, K.; Olson, K. R.; Mecham, S. J.; Devaux, D.; Desimone, J. M.; Balsara, N. P. Relationship between Conductivity, Ion Diffusion, and Transference Number in Perfluoropolyether Electrolytes. *Macromolecules* **2016**, *49* (9), 3508−3515.
(59) Pesko, D. M.; Timachova, K.; Bhattacharya, R.; Smith, M. C.; Villaluenga, I.; Newman, J.; Balsara, N. P. Negative Transference Numbers in Poly(Ethylene Oxide)-Based Electrolytes. *J. Electrochem. Soc.* **2017**, *164* (11), E3569−E3575.
(60) Balsara, N. P.; Newman, J. Relationship between Steady-State Current in Symmetric Cells and Transference Number of Electrolytes Comprising Univalent and Multivalent Ions. *J. Electrochem. Soc.* **2015**, *162* (14), A2720−A2722.
(61) Pallister, P. J.; Moudrakovski, L.; Ripmeester, J. A. Mg-25 Ultra-High Field Solid State NMR Spectroscopy and First Principles Calculations of Magnesium Compounds. *Phys. Chem. Chem. Phys.* **2009**, *11*, 11487−11500.
(62) Kumar, G.G.; Munichandraiah, N. Reversibility of Mg/Mg2+ Couple in a Gel Polymer Electrolyte. *Electrochim. Acta* **1999**, *44*, 2663−2666.
(63) Aurbach, D.; Gofer, Y.; Lu, Z.; Schechter, A.; Chusid, O.; Gizbar, H.; Cohen, Y.; Ashkenazi, V.; Moshkovich, M.; Turgeman, R.; Levi, E. A Short Review on the Comparison between Li Battery Systems and Rechargeable Magnesium Battery Technology. *J. Power Sources* **2001**, *97*−*98*, 28−32.
(64) Tutusaus, O.; Mohtadi, R.; Singh, N.; Arthur, T. S.; Mizuno, F. Study of Electrochemical Phenomena Observed at the Mg Metal/Electrolyte Interface. *ACS Energy Lett.* **2017**, *2*, 224−229.
(65) Son, S.-B.; Gao, T.; Harvey, S. P.; Steirer, K. X.; Stokes, A.; Norman, A.; Wang, C.; Cresce, A.; Xu, K.; Ban, C. An Artificial Interphase Enables Reversible Magnesium Chemistry in Carbonate Electrolytes. *Nat. Chem.* **2018**, *10*, 532−539.
(66) Fu, K. K.; Gong, Y.; Liu, B.; Zhu, Y.; Xu, S.; Yao, Y.; Luo, W.; Wang, C.; Lacey, S. D.; Dai, J.; Chen, Y.; Mo, Y.; Wachsman, E.; Hu, L. Toward Garnet Electrolyte−Based Li Metal Batteries: An Ultrathin, Highly Effective, Artificial Solid-State Electrolyte/Metallic Li Interface. *Sci. Adv.* **2017**, *3* (4), 1−12.

DOI: 10.1021/acsaem.9b01455
ACS Appl. Energy Mater. 2019, 2, 7980−7990

(67) Tchitchekova, D. S.; Monti, D.; Johansson, P.; Ponrouch, A.; Bardé, F.; Randon-Vitanova, A.; Palacín, M. R.; Tchitchekova, D. S. On the Reliability of Half-Cell Tests for Monovalent (Li+, Na+) and Divalent (Mg2+, Ca2+) Cation Based Batteries. *J. Electrochem. Soc.* **2017**, *164* (7), A1384−A1392.
(68) Yan, C.; Yang, H.; Zhao, Y.; Yang, X.; Wang, X.; Schultz, J. M.; Wang, S.; Wang, H. Preparation of Gamma-PVDF with Controlled Orientation and Insight into Phase Transformation. *Polymer* **2017**, *123*, 282−289.
(69) Shanthi, P.; Hanumantha, P.; Albuquerque, T.; Gattu, B.; Kumta, P. N. Novel Composite Polymer Electrolytes of PVdF-HFP Derived by Electrospinning with Enhanced Li-Ion Conductivities for Rechargeable Lithium−Sulfur Batteries. *ACS Appl. Energy Mater.* **2018**, *1* (2), 483−494.
(70) Plimpton, S. Fast Parallel Algorithms for Short-Range Molecular Dynamics. *J. Comput. Phys.* **1995**, *117*, 1−19.
(71) Chaban, V. V.; Voroshylova, I. V. Systematic Refinement of Canongia Lopes-Pádua Force Field for Pyrrolidinium-Based Ionic Liquids. *J. Phys. Chem. B* **2015**, *119* (20), 6242−6249.
(72) Canongia Lopes, J. N.; Deschamps, J.; Pádua, A. A. H. Modeling Ionic Liquids Using a Systematic All-Atom Force Field. *J. Phys. Chem. B* **2004**, *108* (6), 2038−2047.
(73) Lachet, V.; Teuler, J. M.; Rousseau, B. Classical Force Field for Hydrofluorocarbon Molecular Simulations. Application to the Study of Gas Solubility in Poly(Vinylidene Fluoride). *J. Phys. Chem. A* **2015**, *119* (1), 140−151.
(74) Agieienko, V. N.; Kolesnik, Y. V.; Kalugin, O. N. Structure, Solvation, and Dynamics of Mg2+, Ca2+, Sr2+, and Ba2+ Complexes with 3-Hydroxyflavone and Perchlorate Anion in Acetonitrile Medium: A Molecular Dynamics Simulation Study. *J. Chem. Phys.* **2014**, *140* (19), 194501.
(75) Wang, M.; Yu, J.; Lin, S. Lithiation-Assisted Strengthening Effect and Reactive Flow in Bulk and Nanoconfined Sulfur Cathodes of Lithium-Sulfur Batteries. *J. Phys. Chem. C* **2017**, *121* (31), 17029−17037.
(76) Wang, M.; Yuwono, J. A.; Vasudevan, V.; Birbilis, N.; Medhekar, N. V. Atomistic Mechanisms of Mg Insertion Reactions in Group XIV Anodes for Mg-Ion Batteries. *ACS Appl. Mater. Interfaces* **2019**, *11*, 774−783.

DOI: 10.1021/acsaem.9b01455
ACS Appl. Energy Mater. 2019, 2, 7980−7990